XPS Demonstration of $\pi-\pi$ Interaction between Benzyl Mercaptan and Multiwalled Carbon Nanotubes and Their Use in the Adhesion of Pt Nanoparticles

D.-Q. Yang, B. Hennequin, and E. Sacher*

Regroupement Québécois de Matériaux de Pointe, Département de Génie Physique, École Polytechnique, C.P. 6079, succursale Centre-Ville, Montréal, Québec H3C 3A7, Canada

Received May 30, 2006. Revised Manuscript Received August 14, 2006

We have carried out the functionalization of multiwalled carbon nanotubes (MWCNTs) via $\pi-\pi$ interaction with benzyl mercaptan. The presence of noncovalently bonded benzyl mercaptan was demonstrated by X-ray photoelectron spectroscopy, which revealed spectral changes indicating its $\pi-\pi$ interaction with the CNTs. The subsequent bonding of the thiol groups to both evaporated and chemically reduced Pt nanoparticles was demonstrated by the formation of strong Pt−S bonds in the Pt 4f and S 2p spectra. High-resolution transmission electron microscopy was used to confirm the Pt nanoparticle distribution along the walls of the CNTs.

Introduction

Many applications utilizing carbon nanotubes (CNTs, which can exist as single-walled, SWCNTs, or multiwalled, MWCNTs) require the surface to be functionalized in order to participate in chemical or physical reactions. For example, the generation of high-strength fibers or CNT composites is associated with the separation of as-formed CNT bundles into individual CNTs and their subsequent thermodynamically stable dispersion in a polymer matrix. Load transfer efficiency demands that nanotube surfaces be thermodynamically compatible with the host matrix.[1] Further, sensor applications involve the tethering of chemical moieties with specific recognition sites for analytes to nanotube surfaces to ensure the observation of a predictable response in the optical or transport properties of the CNTs.[2] In addition, in the case of metal nanoparticles deposited onto CNTs serving as high-surface-area catalysts in industrial processes, CNT functionalization[3−6] is needed for strong interfacial interactions, so as to obtain and maintain both a larger ratio between the metal nanoparticle surface and volume and an increased nanoparticle loading. The ability to control the type of functionalization permits the tailoring of physical and chemical properties for specific applications.

Many methods have been used for CNT functionalization, including (1) wet chemical processing and (2) dry chemical processing. Wet chemical processing comprises oxidation in strong acids and subsequent derivatization;[7,8] direct reaction with fluorine and subsequent nucleophilic substitution;[9,10] electrochemical or thermal reduction of aryl diazonium salts;[11,12] addition of radicals, nitrenes, or carbenes;[13] supramolecular complexation with detergents, proteins, or polymers;[14−16] ozonolysis and subsequent derivatization;[17−19] ultrasonication with organic materials;[20] and, recently, thiolation with elemental sulfur.[21] Dry chemical processing comprises plasmas using both nonreactive and reactive gases[22−24] and low-energy ion-beam bombardment in a vacuum.[25]

These methods involve both covalent and noncovalent (e.g., $\pi-\pi$ interaction[26−29]) bonding; a $\pi-\pi$ interaction was

* To whom correspondence should be addressed. E-mail: edward.sacher@polymtl.ca. Tel.: (514)340-4711, ext. 4858. Fax. (514)340-3218.

(1) Calvert, P. *Nature* **1999**, *399*, 210.
(2) Dai, H. *Acc. Chem. Res.* **2002**, *35*, 1035.
(3) Toda, T.; Igarashi, H.; Uchida, H.; Watanabe, M. *J. Electrochem. Soc.* **1999**, *146*, 3750.
(4) Springer, T. E.; Zawodzinski, T. A.; Gottesfeld, S. *J. Electrochem. Soc.* **1991**, *138*, 2334.
(5) Service, R. *Science* **2002**, 296, 1222.
(6) Sun, X.; Stansfield, B. L.; Dodelet, J. P.; Désilets, S. *Chem. Phys. Lett.* **2002**, *363*, 415.
(7) Chen, J.; Hamon, M. A.; Hu, H.; Chen, Y.; Rao, A. M.; Eklund, P. C.; Haddon, R. C. *Science* **1998**, *282*, 95.
(8) Liu, J.; Rinzler, A. G.; Dai, H.; Hafner, J. S.; Bradley, R. K.; Boul, P. J.; Lu, A.; Iverson, T.; Shelimov, K.; Huffman, C. B.; Rodriguez-Macias, F.; Shon, Y.; Lee, T. R.; Colbert, D. T.; Smalley, R. E. *Science* **1998**, *280*, 1253.
(9) Mickelson, E. T.; Hoffman, C. B.; Rinzler, A. G.; Smalley, R. E.; Hauge, R. H.; Margrave, J. L. *Chem. Phys. Lett.* **1998**, *296*, 188.
(10) Boul, P. J.; Liu, J.; Mickelson, E. T.; Huffman, C. B.; Ericson, L. M.; Chiang, I. W.; Smith, K. A.; Colbert, D. T.; Hauge, R. H.; Margrave, J. L.; Smalley, R. E. *Chem. Phys. Lett.* **1999**, *310*, 367.
(11) Bahr, J. L.; Yang, J.; Kosynkin, D. V.; Bronikowski, M.; Smalley, R. E.; Tour, J. M. *J. Am. Chem. Soc.* **2001**, *123*, 6536.
(12) Bahr, J. L.; Tour, J. M. *Chem. Mater.* **2001**, *13*, 3823.
(13) Holzinger, M.; Vostrowskv, O.; Hirsch, A.; Hennrich, F.; Kappes, M.; Weiss, R.; Jellen, F. *Angew. Chem., Int. Ed.* **2001**, *40*, 4002.
(14) Chen, R. J.; Zhang, Y.; Wang, D.; Dai, H. *J. Am. Chem. Soc.* **2001**, *123*, 3838.
(15) Chen, R. J.; Bangsaruntip, S.; Drouvalakis, K. A.; Kam, N. W. S.; Shim, M.; Li, Y.; Kim, W.; Utz, P. J.; Dai, H. *Proc. Natl. Acad. Sci. U.S.A.* **2003**, *100*, 4984.
(16) Star, A.; Stoddart, J. F.; Steuerman, D.; Diehl, M.; Boukai, A.; Wong, E. W.; Yang, X.; Chung, S.; Choi, H.; Heath, J. R. *Angew. Chem., Int. Ed.* **2001**, *40*, 1721.
(17) Mawhinney, D. B.; Naumenko, V.; Kuznetsova, A.; Yates, J. T.; Liu, J.; Smalley, R. E. *J. Am. Chem. Soc.* **2000**, *122*, 2383.
(18) Cai, L.; Bahr, J. L.; Yao, Y.; Tour, J. M. *Chem. Mater.* **2002**, *14*, 4235.
(19) Banerjee, S.; Wong, S. S. *J. Phys. Chem. B* **2002**, *106*, 12144.
(20) Koshio, A.; Yudasaka, M.; Zhang, M.; Iijima, S. *Nano Lett.* **2001**, *7*, 361.
(21) Khare, B. N.; Meyyappan, M.; Cassell, A. M.; Nguyen, C. V.; Han, J. *Nano Lett.* **2002**, *2*, 73.

10.1021/cm061256s CCC: $33.50
Published on Web 09/19/2006

originally proposed[30] as an explanation for the attractive interaction that exists between molecules containing π orbitals in the absence of spectroscopic evidence for HOMO−LUMO interactions. A $\pi-\pi$ interaction is an electrostatic interaction in which the offset and/or orientation of the π orbitals on opposing molecules maximizes the opposing $\sigma-\pi$ attractive interactions while minimizing the opposing $\pi-\pi$ repulsive interactions. Such interactions with CNTs can be surprisingly strong, depending on the opposing molecules, capable of withstanding temperatures of >400° C.[31] Manifesting fewer detrimental effects on the electrical and mechanical properties of CNTs, these latter methods have attracted considerable attention.[8]

Pt nanoparticles supported on CNTs have attracted interest as fuel-cell cathode electrocatalysts for oxygen reduction at relatively low temperatures[32−39] and as electrochemical biosensing platforms[40] because of the very large surface-to-volume ratio of the CNTs. However, it is difficult to control the Pt nanoparticle loading,[36] as well as their dimensions and densities. There is also a serious nanoparticle adhesion problem because Pt interacts weakly with pristine CNTs; this permits nanoparticle surface diffusion and coalescence, strongly affecting catalytic efficiency. One must choose an appropriate CNT surface modification, e.g., grafted chemical groups,[32−39] to increase the interaction with the Pt nanoparticles, to control their dimensions and densities. Surface chemistry also strongly affects metal quantum-dot dimensions, shapes, and densities[41] and metal/CNT composite mechanical properties,[42] as well as the electrical contact properties of metal/CNT-based devices.[43] The catalytic efficiency of supported Pt nanoparticles[39] has been found to increase with the extent of dispersion, as well as with a narrow size distribution between 2 and 4 nm.

As recently reported,[36] a potential CNT functionalization method for achieving this efficiency is the thiolation of CNTs, to form S−Pt covalent bonds. Although sulfur is generally recognized to be a surface poison that decreases electrocatalytic activity, it was shown by Kim and Mitani[36] that there is no such effect of the sulfur of thiol groups on Pt−CNTs, in either methanol oxidation (MOR) or oxygen reduction (ORR) reactions, when there is strong adhesion of the S-containing moiety to the CNT.

Here, we explore such thiolation through the surface functionalization of MWCNTs with benzyl mercaptan ($C_6H_5-CH_2-SH$) as an example of thiolation through a $\pi-\pi$ interaction. Similar interactions are expected with other aromatic thiols, differing only in the surface density of the grafted thiol groups (size effect) and the thermal stability of the $\pi-\pi$ interaction.[31] In the case of benzyl thiol, the phenyl ring (C_6H_5-) participates in a $\pi-\pi$ interaction with the walls of the CNTs, and the thiol group (−SH), separated from the phenyl ring by a methylene group ($-CH_2-$) to minimize electron delocalization between the two, is intended to react with the Pt nanoparticle through the formation of a S−Pt bond. We have chosen to use benzyl mercaptan because the small dimensions of the phenyl ring permit (a) a high density of thiol groups on the CNTs and (b) a shorter electrical contact distance between the Pt nanoparticle and the CNT; benzyl mercaptan is also readily available and easy to use. The thiolation process was followed by both X-ray photoelectron spectroscopy (XPS) and high-resolution transmission electron microscopy (HRTEM). Despite the fact that spectroscopic evidence for a $\pi-\pi$ interaction is normally lacking, which results in such an interaction being assumed rather than demonstrated, we show that XPS spectral evidence exists that clearly confirms such interaction.

Experimental Section

MWCNTs (95% purity, 20−30-nm diameter, 1−5-μm length) were obtained from Nano-Lab, Brighton, MA; 0.5 mg of the CNTs was dispersed in 5 mL of 18 MΩ deionized water and sonicated for 1 h to separate the nanotubes.[25,29] They were then mixed with 375 μL of benzyl mercaptan dissolved in 1175 μL of ethanol, and the solution was sonicated for 30 min or less. (XPS has revealed that sonication for longer times causes significant thiol oxidation.) A well-dispersed CNT mixture was obtained, that was stable for several days.

For XPS analysis, the mixture was deposited onto a piece of Si wafer by dropping and drying. XPS analysis was carried out in a VG ESCALAB 3 Mark II apparatus, using nonmonochromated Mg Kα radiation at 300 W. The instrument resolution was ~0.75 eV. The instrument analysis chamber is directly attached to a UHV preparation chamber via a gate valve, avoiding air exposure upon sample transfer. Pt nanoparticles were deposited either by evaporation in the preparation chamber, with an electron-beam evaporator, using a deposition rate of 0.15 nm/min at a pressure of 2×10^{-8}

(22) Plank, N. O. V.; Jiang, L.; Cheung, R. *Appl. Phys. Lett.* **2003**, *83*, 2426.
(23) Khare, B. N.; Wilhite, P.; Quinn, R. C.; Chen, B.; Schingler, R. H.; Tran, B.; Imanaka, H.; So, C. R.; Bauschlicher, C. W.; Meyyappan, M. *J. Phys. Chem. B* **2004**, *108*, 8166.
(24) Plank, N. O. V.; Cheung, R.; Andrews, R. J. *Appl. Phys. Lett.* **2004**, *85*, 3229.
(25) Yang, D.-Q.; Rochette, J.-F.; Sacher, E. *Langmuir* **2005**, *21*, 8539.
(26) Chen, R. J.; Zhang, Y. G.; Wang, D. W.; Dai, H. *J. Am. Chem. Soc.* **2001**, *123*, 3838.
(27) Nakashima, N.; Tomonari, Y.; Murakami, H. *Chem. Lett.* **2002**, *31*, 638.
(28) Yang, D.-Q.; Rochette, J.-F.; Sacher, E. *J. Phys. Chem. B* **2005**, *109*, 4481.
(29) Yang, D.-Q.; Rochette, J.-F.; Sacher, E. *J. Phys. Chem. B* **2005**, *109*, 7788.
(30) Hunter, C. A.; Sanders, J. K. M. *J. Am. Chem. Soc*. **1990**, *112*, 5525.
(31) Lee, Y.; Song, H. J.; Shin, H. S.; Shin, H. J.; Choi, H. C. *Small* **2005**, *1*, 975.
(32) Che, G. L.; Lakshmi, B. B.; Fisher, E. R.; Martin, C. R. *Nature* **1998**, *393*, 346.
(33) Rodriguez, N. M.; Kim, M.-S.; Baker, R. T. K. *J. Phys. Chem*. **1994**, *98*, 13108.
(34) Toda, T.; Igarashi, H.; Uchida, H.; Watanabe, M. *J. Electrochem. Soc.* **1999**, *146*, 3750.
(35) Girishkumar, G.; Vinodgopal, K.; Kamat, P. V. *J. Phys. Chem. B* **2004**, *108*, 19960.
(36) Kim, Y.-T.; Ohshima, K.; Higashimine, K.; Uruga, T.; Takata, M.; Suematsu, H.; Mitani, T. *Angew. Chem., Int. Ed.* **2006**, *45*, 407. Kim, Y.-T.; Mitani, T. *J. Catal.* **2006**, *238*, 394.
(37) Mu, Y. Y.; Liang, H. P.; Hu, J. S.; Jiang, L.; Wan, L. J. *J. Phys. Chem. B* **2005**, *109*, 22212.
(38) Hull, R. V.; Li, L.; Xing, Y. C.; Chusuei, C. C. *Chem. Mater*. **2006**, *18*, 1780.
(39) Waje, M. M.; Wang, X.; Li, W. Z.; Yan, Y. S. *Nanotechnology* **2005**, *16*, S395.
(40) Hrapovic, S.; Liu, Y. L.; Male, K. B.; Luong, J. H. T. *Anal. Chem.* **2004**, *76*, 1083.
(41) Azamian, B. R.; Coleman, K. S.; Davis, J. J.; Hanson, N.; Green, M. L. H. *Chem. Commun.* **2002**, 366.
(42) Zhao, Q.; Nardelli, M. B.; Lu, W.; Bernholc, J. *Nano Lett.* **2005**, *5*, 847.
(43) Zhong, J.-X.; Stocks, G. M. *Appl. Phys. Lett.* **2005**, *87*, 133105.

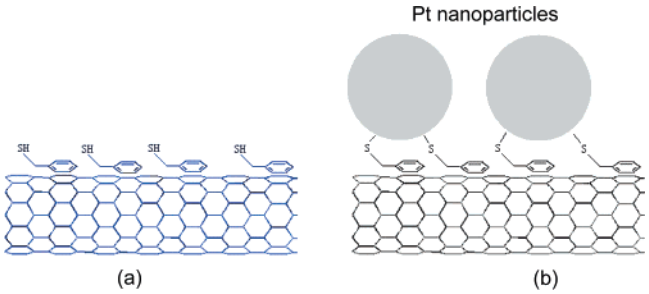

Figure 1. Schematics of (a) a CNT functionalized with benzyl mercaptan via $\pi-\pi$ bonding and (b) the bonding of Pt nanoparticles to the functionalized CNT via covalent S−Pt bond formation.

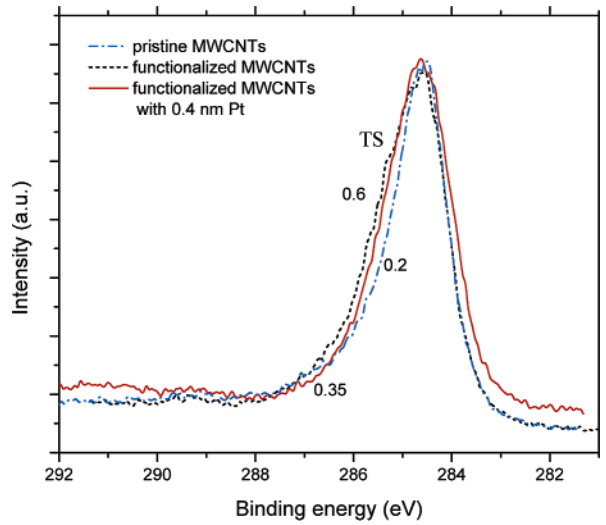

Figure 2. C 1s XPS spectral line shape comparison of MWCNTs: (a) pristine MWCNTs, (b) after benzyl mercaptan functionalization, and (c) after evaporation of 0.4 nm of Pt onto the functionalized MWCNTs.

Torr (the base pressure in the deposition chamber was $<1 \times 10^{-9}$ Torr) or by the addition of separately produced nanoparticles, prepared by the wet chemical reduction of equal volumes of 0.03 M aqueous H_2PtCl_6 by 0.1 M HCOOH. After Shirley background subtraction, the spectra were analyzed by the XPSPeak 4.1 program.[44] This freely available program uses two terms, TS and TL, to express asymmetry; the value of TS controls the peak asymmetry (TS = 0 for a symmetric peak), and the value of TL controls the tail asymmetry.

For HRTEM analysis, the mixture was deposited onto a 400-mesh Cu grid by dropping and drying. Pt was evaporated onto the HRTEM sample using a separate electron-beam evaporator at a pressure of 10^{-7} Torr. HRTEM was carried out in a JEOL JEM-2100F instrument operating at 200 keV, using a high-brightness LaB_6 electron gun.

Results and Discussion

Figure 1 presents a schematic of benzyl mercaptan attached to CNTs via a $\pi-\pi$ interaction. In the absence of obvious spectroscopic changes,[30,31] the following evidence attests to the presence of this interaction:

(1) The C 1s XPS core-level spectra are seen in Figure 2. The C 1s line shape is observed to change in the following ways:

(a) The TS asymmetry index increases from 0.2 (untreated CNTs) to 0.6 (after benzyl mercaptan functionalization). As we previously demonstrated for both HOPG[45] and CNTs,[25] the C 1s spectrum is composed of five components, one of which, C2, at 285.6 eV, represents electron delocalization whose range has been limited for some reason (e.g., structural damage, chemical interaction). We have shown[43] that the value of the TS asymmetry index correlates with the intensity of the C2 peak when the alternant hydrocarbon structure was intentionally damaged by an Ar^+ beam.[44] In the present case, a $\pi-\pi$ interaction with the extensively delocalized undamaged structure, represented by the C1 component of the C 1s spectrum at 284.6 eV,[46,47] effectively limits the delocalization, increasing the C2/C1 intensity ratio in the C 1s spectrum; this is demonstrated by the measured increase in the TS asymmetry index.[45]

(b) There is also an increase of the C 1s spectral peak width upon functionalization, from 1.3 to 1.7 eV. This is expected when the electron delocalization becomes limited[45,46] as a result of the interaction of benzyl mercaptan with the CNT sidewall. Broadening is also due to the overlapping of the CNT and benzyl mercaptan C 1s spectral envelopes, which causes an increased intensity in the binding energy region around 286.5 eV (C−SH). Both contributions are manifested as slight increases in peak width and asymmetry.

(2) The functionalized CNTs are remarkably stable, with no obvious change in their S 2p XPS spectrum, when kept under UHV at room temperature for several days, when annealed under UHV at 100 °C for 1 h, or when washed repeatedly with water. Even after several days at room temperature, the relative concentration of S is about 5%, although the fact that our CNTs are multiwalled prevents our determination of surface coverage. However, we can *estimate* the coverage from the following data: The sonochemical oxidation of similar CNTs in strong acid gave an oxygen concentration of 8−10%.[38,47] The assumption was made that the surface was saturated with oxidation products (i.e., C−OH, C═O, and COOH). Considering both the CNT/benzyl mercaptan orientation in Figure 1a and the relatively larger size of the phenyl ring, a 5% relative concentration of S implies saturation by benzyl mercaptan. This estimate is supported by the TEM photomicrographs to be discussed later.

(3) Upon deposition of a nominal 0.4 nm of Pt, both the TS peak asymmetry index and the width of the C 1s spectrum decrease (Figure 2), as a result of charge transfer as the S forms a polarized Pt−S bond.

(4) The variations of the S 2p and Pt 4f peak line shapes in Figures 3 and 4, respectively, upon Pt nanoparticle deposition suggest a $\pi-\pi$ interaction as follows:

(a) S 2p spectra have an S $2p_{3/2,1/2}$ doublet structure. All of our spectra were fit using the expected 2:1 peak area ratio and a 1.2-eV peak separation, as shown in Figure 3. The S $2p_{3/2}$ peak is located at 163.5 eV (Figure 3a) upon thiol functionalization,[48] a binding energy attributed to C−SH bonds,

(44) http://www.uksaf.org/software.html (accessed April 2004).

(45) Yang, D.-Q.; Sacher, E. *Surf. Sci.* **2002**, *504*, 125.
(46) Yang, D.-Q.; Sacher, E. *Langmuir* **2006**, *22*, 860.
(47) Xing, Y. C.; Li, L.; Chusuei, C. C.; Hull, R. V. *Langmuir* **2005**, *21*, 4185.
(48) Volmer, M.; Stratmann, M.; Viefhaus, H. *Surf. Interface Anal.* **1990**, *16*, 278.

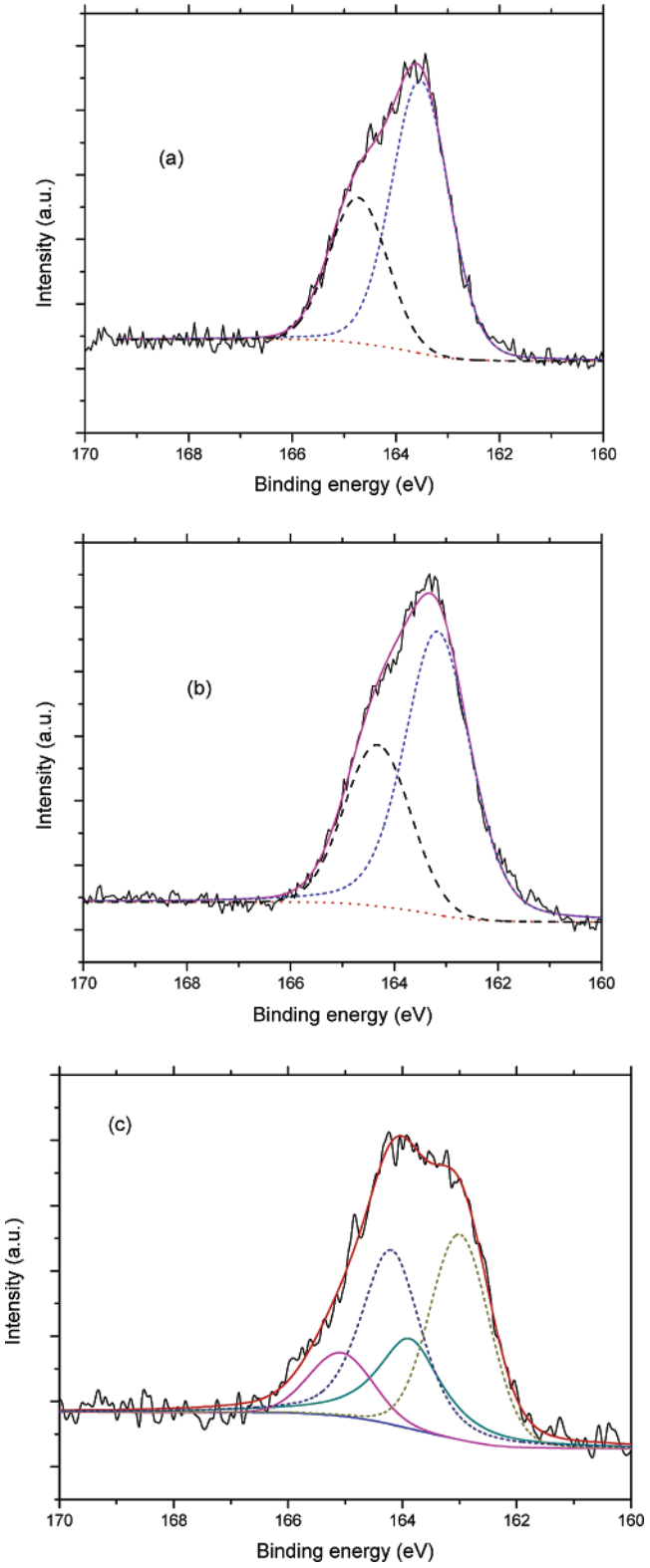

Figure 3. S 2p XPS spectra of functionalized CNTs (a) before and (b,c) after deposition of a nominal 0.4 nm of Pt by (b) evaporation and (c) chemical reduction.

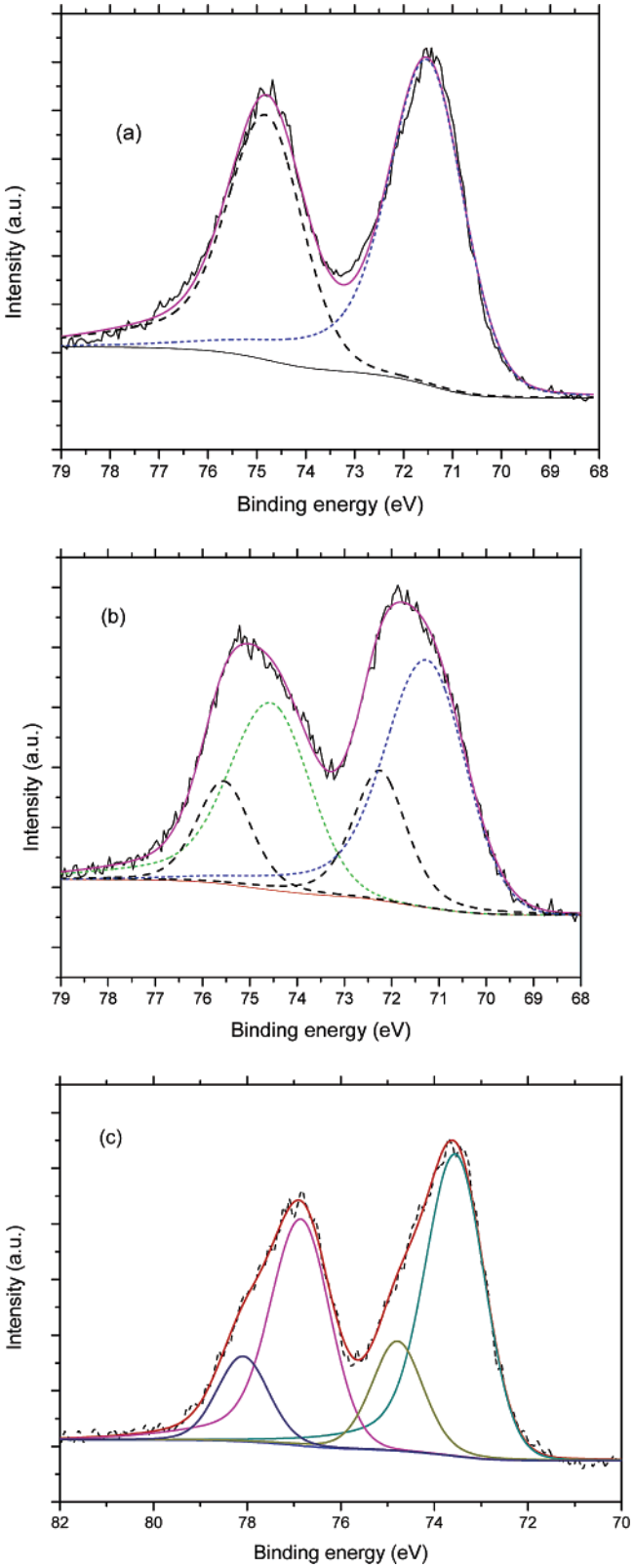

Figure 4. Pt 4f XPS spectra of (a) pristine and (b,c) functionalized CNTs after deposition of a nominal 0.4 nm of Pt by (b) evaporation and (c) chemical reduction.

and is shifted to 163.2 and 163.0 eV, respectively, upon Pt deposition by evaporation (Figure 3b) and upon the addition of chemically reduced nanoparticles (Figure 3c), as polar Pt−S bonds (the low-binding-energy components in Figure 3b,c) are formed. The component at higher binding energy represents thiol bonded to CNTs but not bonded to Pt.

(b) Pt 4f spectra also have a doublet structure, Pt $4f_{7/2,5/2}$. All of our spectra were fit with the expected 4:3 peak area ratio and a 3.3-eV peak separation, as seen in Figure 4. As found by others[49] and recently confirmed by us,[50] Pt 4f peaks

(49) Cheung, T. T. *Surf. Sci.* **1984**, *140*, 151.

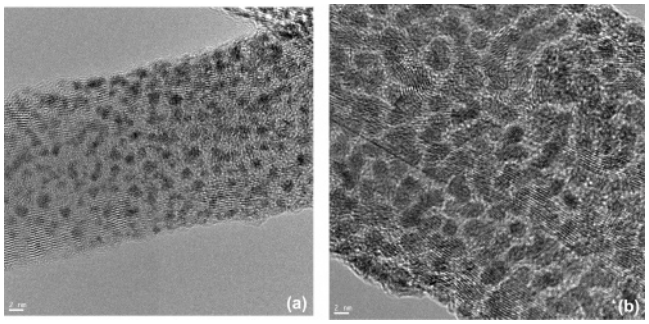

Figure 5. HRTEM photomicrographs of a nominal 1 nm of *evaporated* Pt on (a) pristine and (b) functionalized MWCNTs.

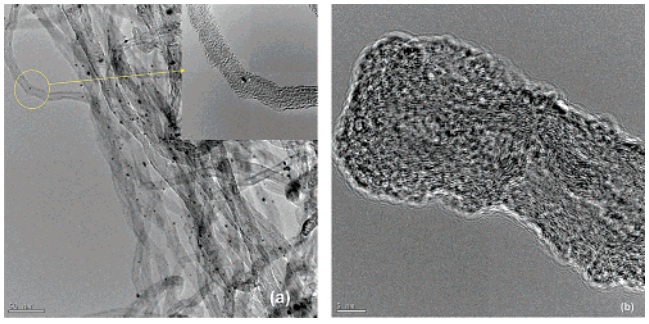

Figure 6. HRTEM photomicrographs of *chemically reduced* Pt nanoparticles on (a) pristine and (b) functionalized MWCNTs. Different scales are used in a and b for clarity.

are asymmetric, and an asymmetry index was used in peak separation in the present case. Figure 4a shows the spectrum of Pt that has been deposited onto pristine CNTs, with which it does not react chemically; Figure 4b shows the same spectrum for Pt that has been deposited onto functionalized CNTs. A comparison demonstrates the presence of the Pt−S bond, manifested by the $2p_{3/2}$ peak located at 72.3 eV (Pt^0, from the nanoparticle bulk, is located 71.3 eV), indicating a positively charged species, in agreement with reported values.[51,52] The lower-energy components represent Pt in the nanoparticle that is not in contact with the thiol and has, therefore, not formed a bond to S.

There is some difference for chemically reduced Pt samples: As seen in Figure 4c, a somewhat larger shift in binding energy is observed for the Pt 4f spectrum, which consists of two contributions, with the Pt $4f_{7/2}$ peaks located at 73.6 and 74.8 eV. These are almost 2.3 eV higher than that of the evaporated Pt. This unexpected higher binding energy can be attributed to both larger final-state effects, because of the extremely small size of the nanoparticles[53] (as confirmed by our HRTEM photomicrographs, shown later), and nanoparticle charging due to a loss of conductivity as the Kubo gap increases with diminishing nanoparticle size.[53] It is noted that the S 2p binding energy for this case, in Figure 3c, is also slightly shifted to higher binding energy, as mentioned in section 4a above. In addition, a higher binding energy indicates the presence of partially reduced Pt, which would be expected to be nonconductive. It is our experience that, if left sufficiently long in the reducing medium, further reduction occurs, to ultimately give essentially pure Pt^0.

Unfortunately, when chemically reduced Pt nanoparticles are mixed with untreated CNTs, too little Pt adheres to be analyzed by XPS. However, when an aqueous dispersion of chemically reduced Pt nanoparticles is dropped onto a surface-oxidized Si wafer and permitted to dry, its Pt 4f spectrum is identical to that of Pt evaporated onto the same Si wafer, as well as onto HOPG,[50] where it is known to be Pt^0.

Figure 5 shows an HRTEM photomicrographic comparison of a nominal 1-nm-thick Pt deposit *evaporated* onto pristine (Figure 5a) and functionalized (Figure 5b) CNTs. Clearly, little Pt (estimated coverage, 30%, with a nanoparticle size of 1.2 ± 0.1 nm) has been deposited onto the pristine CNT surface in Figure 5a, some of which is certainly due to the presence of defects. However, a significantly enhanced Pt nucleation density is observed on the functionalized CNTs in Figure 5b, where the Pt coverage has reached more than an estimated 65%, with a very narrow nanoparticle distribution of 2.1 ± 0.2 nm. This extent of coverage and size distribution is the greatest we have ever found, no matter which treatment we used to functionalize the CNTs (e.g., Ar plasma treatment and defect creation by ion beam[54]). The present functionalization treatment also appears to furnish a surface that is better wet by the Pt (Figure 5b).

The very low Pt coverage for evaporated Pt on pristine CNTs (Figure 5a) is due to a low sticking coefficient because of a low concentration of widely separated nucleation sites (defects in the case of pristine CNTs). Functionalization (Figure 5b) introduces thiol groups along the sidewalls of the CNTs, resulting in a high concentration of closely spaced nucleation sites.

The interaction of Pt nanoparticles with untreated CNTs, similar to that with untreated HOPG, is weak,[35] leading to poor wetting of the evaporated Pt. This causes Pt to have a very low nucleation density in both cases. However, there are differences between depositing evaporated Pt onto CNTs and HOPG: (a) the nucleation density is greater on CNTs and exhibits good uniformity, indicating the presence of a higher concentration of surface defects, which is consistent with XPS C 1s peak shape analyses,[46,50] and (b) the size of our Pt nanoparticles on pristine CNTs on TEM grids is smaller. We believe this to be due to a weaker Pt−CNT interaction, leading to a lower Pt sticking coefficient. We note that the suspended CNTs offer a limited surface area for the coalescence of depositing Pt atoms, which might be a major reason for the difference in Pt morphologies on HOPG and suspended pristine CNTs.

Figure 6 shows a similar comparison of *chemically reduced* Pt deposited onto pristine (Figure 6a) and functionalized (Figure 6b) CNTs. The morphology is clearly different than that in Figure 5. The Pt nanoparticle density on the pristine surface is significantly lower (Figure 6a, inset), with ~2-nm nanoparticles, because of the weak interaction. In

(50) Yang, D.-Q.; Zhang, G.-X.; Sacher, E. *J. Phys. Chem. B* **2006**, *110*, 8348.
(51) Grim, S. O.; Matienzo, L. J.; Swartz, W. E. *Inorg. Chem.* **1974**, *13*, 447.
(52) Roundhill, D. M.; Brant, P.; Walton, R. A.; Feltham, R. D.; Best, S. A.; Rauchfuss, T. B. *Inorg. Chem.* **1977**, *16*, 1976.
(53) Eberhardt, W.; Fayet, P. *Phys. Rev. Lett.* **1990**, *64*, 780.
(54) Yang, D.-Q.; Sacher, E., manuscript to be submitted.

contrast, Pt nanoparticles, <1 nm in size, almost completely cover the functionalized CNTs sidewall, indicating a strong interaction with the functionalized CNT surface. The very strong Pt−S covalent bond restricts Pt surface diffusion, and as a result, the nanoparticles cannot coalesce into the larger particles seen in Figure 6a. A comparison of functionalized CNTs, uniformly decorated with both evaporated and chemically reduced Pt nanoparticles (Figures 5b and 6b), indicates that the functionalization achieved here, through a $\pi-\pi$ interaction, is both uniform and highly dense.

The nanoparticles produced by chemical reduction and deposited onto functionalized CNTs are too small to have catalytic activity;[55] larger Pt nanoparticles (e.g., 2−4 nm) are needed for such activity. Such particles must be produced before deposition because, once deposited onto functionalized CNTs, they can no longer diffuse and coalesce. We are presently pursuing the optimization of nanoparticle size produced through chemical reduction.

(55) Rao, C. N. R.; Kulkarni, G. U.; Thomas, P. J.; Edwards, P. P. *Chem. Eur. J.* **2002**, *8*, 28. Greeley, J.; Norskøv, J. K.; Mavrikakis, M. *Annu. Rev. Phys. Chem.* **2002**, *53*, 319.

Conclusions

We have successfully functionalized MWCNTs with thiol groups via a $\pi-\pi$ interaction with benzyl mercaptan. The functionalized CNT surface interacts strongly with Pt nanoparticles through the formation of Pt−S bonds and results in a very high Pt nanoparticle loading (both high dispersion and narrow size distribution). This method can also be used for SWCNT surface functionalization, to improve Pt nanoparticle adhesion and loading and to better control their dimensions.

Acknowledgment. We thank the Natural Sciences and Engineering Research Council of Canada and GM Canada for funding.

CM061256S